JACS
JOURNAL OF THE AMERICAN CHEMICAL SOCIETY
pubs.acs.org/JACS
Article

Blending Ionic and Coordinate Bonds in Hybrid Semiconductor Materials: A General Approach toward Robust and Solution-Processable Covalent/Coordinate Network Structures

Xiuze Hei,[¶] Wei Liu,[¶] Kun Zhu, Simon J. Teat, Stephanie Jensen, Mingxing Li, Deirdre M. O'Carroll, Kevin Wei, Kui Tan, Mircea Cotlet, Timo Thonhauser, and Jing Li*

Cite This: J. Am. Chem. Soc. 2020, 142, 4242−4253

ABSTRACT: Inorganic semiconductor materials are best known for their superior physical properties, as well as their structural rigidity and stability. However, the poor solubility and solution-processability of these covalently bonded network structures has long been a serious drawback that limits their use in many important applications. Here, we present a unique and general approach to synthesize robust, solution-processable, and highly luminescent hybrid materials built on periodic and infinite inorganic modules. Structure analysis confirms that all compounds are composed of one-dimensional anionic chains of copper iodide ($Cu_mI_{m+2}^{2-}$) coordinated to cationic organic ligands via Cu−N bonds. The choice of ligands plays an important role in the coordination mode (μ^1-MC or μ^2-DC) and Cu−N bond strength. Greatly suppressed nonradiative decay is achieved for the μ^2-DC structures. Record high quantum yields of 85% (λ_{ex} = 360 nm) and 76% (λ_{ex} = 450 nm) are obtained for an orange-emitting 1D-$Cu_4I_6(L_6)$. Temperature dependent PL measurements suggest that both phosphorescence and thermally activated delayed fluorescence contribute to the emission of these 1D-AIO compounds, and that the extent of nonradiative decay of the μ^2-DC structures is much less than that of the μ^1-DC structures. More significantly, all compounds are remarkably soluble in polar aprotic solvents, distinctly different from previously reported CuI based hybrid materials made of charge-neutral Cu_mX_m (X = Cl, Br, I), which are totally insoluble in all common solvents. The greatly enhanced solubility is a result of incorporation of ionic bonds into extended covalent/coordinate network structures, making it possible to fabricate large scale thin films by solution processes.

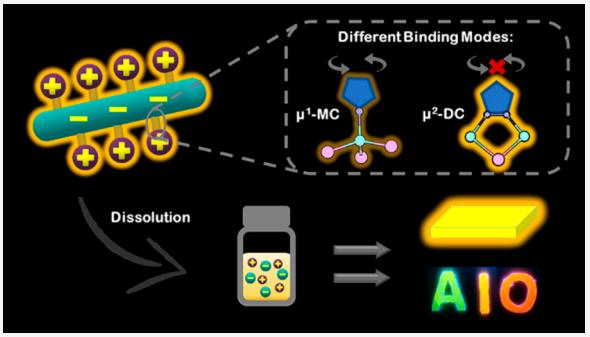

INTRODUCTION

Copper(I) halide based inorganic−organic hybrid semiconductors represent an important class of crystalline materials with unique properties, including structural variety, moisture stability, optical tunability, and strong luminescence.[1−4] In recent years, much attention has been paid to these materials as they show great promise for use as rare-earth element (REE) free phosphors and emissive layers[5] in energy-efficient solid-state lighting (SSL) technology.[6−12] The inorganic motifs of these hybrid structures are charge-neutral Cu_mI_m, which can be zero-dimensional (0D) molecular clusters, one-dimensional (1D) chains, or two-dimensional (2D) layers. They form structures of various dimensionalities (0D−3D) through coordinate bonds with organic ligands.[13,14]

The very interesting and tunable optical properties of this material family are a result of the interplay between the inorganic and organic components. Their photoluminescence (PL) can be attributed to metal-to-ligand charge transfer (MLCT), halide-to-ligand charge transfer (XLCT), cluster centered (CC), or a combination of some of these.[15] The most common inorganic modules in these structures are charge-neutral CuI monomer, Cu_2I_2 rhomboid dimer, Cu_3I_3 trimer, Cu_4I_4 tetramers (cubic and staircase-like), and infinite 1D CuI chains. High photoluminescence quantum yields (PLQYs) or, equivalently, internal quantum yields (IQYs) have been achieved, in some cases approaching those of commercial products. However, one of the major drawbacks is their low blue-light excitability due to the need of a high energy excitation source (e.g., UV light). Strong blue excitability of a phosphor material is required for the current commercial white light-emitting diode (WLED) technology as they use a blue chip as excitation source for phosphors. Another downside is their poor solubility and solution processability, regardless of the type of Cu_mI_m inorganic module (e.g., molecular cluster, chain or layer) and/or dimensionality of the overall structure, a

Received: December 21, 2019
Published: February 11, 2020

https://dx.doi.org/10.1021/jacs.9b13772
J. Am. Chem. Soc. 2020, 142, 4242−4253

common problem to all inorganic solid materials made of covalent/coordinate bonds.

To address these issues, we recently developed a synthetic approach to form molecular structures consisting of covalently bonded cation−anion pairs (0D-AIO structures).[16] Our study demonstrated that both stability and solubility of these molecular species are greatly improved as a result of introducing strong ionic interaction to a coordinated metal and ligand. In addition, suitably chosen ligands with low-lying LUMO energies and strong Cu−N binding energy may enhance their blue-light excitability significantly. In this work, we expand our investigation to compounds made of infinite inorganic anionic chains (i.e., 1D-AIO structures) and benzotriazole based cationic ligands (L). Eight new compounds are synthesized and their crystal structures are determined. They are composed of four different types of copper iodide ($Cu_mI_{m+2}^{2-}$) anionic 1D chains, which bond to organic cationic ligands via two coordination modes, namely, the monocoordination (μ^1-MC) and dicoordination (μ^2-DC). With decomposition temperatures above 190 °C, all compounds are strongly resistant to heat and moisture. Photophysical measurements reveal that the PL performance of the structures bearing μ^2-DC mode is substantially better than those of μ^1-MC mode, with doubled or higher IQY values. A detailed spectroscopic and theoretical analysis has confirmed our hypothesis that more rigid bonds between the inorganic and organic components and the limited ligand vibrations are responsible for the lower nonradiative decay constant (k_{nr}) and stronger luminescence of μ^2-DC structures. IQYs of 85% and 76% are achieved for orange emission (λ_{em}= 596 nm) under UV (λ_{ex} = 360 nm) and blue (λ_{ex} = 450 nm) radiation, respectively. While higher IQYs have been reported for molecular hybrid structures under UV excitation (unsuitable for the current WLED technology),[17−22] the values obtained in this work are the highest among all hybrid structures under blue-light excitation. Notably, all 1D-AIO-$Cu_mI_{m+2}(L)$ compounds are very soluble in polar aprotic solvents despite the infinite nature of the inorganic chains, making them a unique material class having excellent solution processability.

EXPERIMENTAL SECTION

Materials. CuI (98%, Alfa Aesar); $NaNO_2$ (97%, Alfa Aesar); 1*H*-benzo[*d*][1,2,3]triazole (99%, Alfa Aesar); 5-methyl-1*H*-benzotriazole (98%, Sigma-Aldrich); 5,6-dimethyl-1*H*-benzo[*d*][1,2,3]triazole (99%, Sigma-Aldrich); 4-fluoro-1,2-phenylenediamine (97%, Sigma-Aldrich); 1-bromo-3-chloropropane (98%, Alfa Aesar); 1-bromo-4-chlorobutane (99%, Alfa Aesar); 1-bromo-5-chloropentane (98%, Alfa Aesar); 1-bromo-3-chloro-2-methylpropane (98%, TCI); *N*,*N*-dimethylethylamine (99%, Alfa Aesar); *N*,*N*-dimethylisopropylamine (99%, TCI); trimethylamine (33% w/w in ethanol, Alfa Aesar); potassium carbonate (99%, Sigma-Aldrich); potassium iodide (99%, Alfa Aesar); acetone (99.5%, VWR); acetonitrile (99.5%, VWR); ethyl ether (99%, Fisher); sodium salicylate (99%, Merck), $BaMgAl_{10}O_{17}:Eu^{2+}$ and YAG:Ce^{3+} type 9800 (Global Tungsten & Powders Corp), PolyOx N750 (Dow Chemical).

Synthesis of Organic Ligands. All organic ligands are cationic benzotriazole derivatives with different substitute groups. They were prepared according to the reported procedures with some modifications. Typical reactions involved alkylation of one N atom in the aromatic ring. The other two N atoms were left intact and were used as free binding sites to coordinate to copper metals.

Preparation of (1*H*-Benzo[*d*][1,2,3]triazol-1-yl)methanol (*btm*). A mixture of 1*H*-benzo[*d*][1,2,3]triazole (*bta*) (3.4 g, 0.025 mol), distilled water (50 mL), and formaldehyde solution (36%, 10 mL) was first refluxed for 1.5 h. After cooling to room temperature, the resulting white precipitate was collected by filtration, washed with water, and dried under a vacuum to give *btm* as white solid. The yield is 92%.

Preparation of 5-Fluoro-1*H*-benzo[*d*][1,2,3]triazole (*5-F-bta*). 4-Fluoro-1,2-phenylenediamine (5.045 g, 40 mmol) was first dissolved in acetic acid in ice bath. $NaNO_2$ (3.105 g, 45 mmol) in 5 mL DI water was added dropwise while stirring. The reaction mixture was kept stirring under room temperature overnight before the solution was filtered. The solid was purified by recrystallization, giving brown crystalline powder as *5-F-bta*. The yield is 85%.

Preparation of 1-(Chloromethyl)-1*H*-benzo[*d*][1,2,3]triazole (*Cl-mbt*). *Btm* (3.7 g, 0.025 mol) was first dissolved in a mixture of CH_2Cl_2 (60 mL) and dimethylformamide (DMF) (40 mL), and then thionyl chloride (5 mL) in methylene chloride (10 mL) was added dropwise into the reaction mixture under magnetic stirring at room temperature. The reaction mixture was kept stirring for 2 h, then its pH was adjusted by saturated $NaHCO_3$ solution to 7. The organic layer was separated and was evaporated under reduced pressure, giving white crystalline powder as *Cl-mbt*. The yield is 76%.

Preparation of 1-(4-Chlorobutyl)-1*H*-benzo[*d*][1,2,3]triazole (*Cl-bbt*). To 1*H*-benzo[*d*][1,2,3]triazole (*bta*) (3.0 g, 0.025 mol) in acetonitrile (100 mL), K_2CO_3 (4.1 g, 0.030 mol) and 1-bromo-4-chlorobutane (2.9 mL, 0.025 mol) was added. The reaction mixture was stirred for 3 days at room temperature. Then the acetonitrile was removed under reduced pressure, and then the residue was purified by column chromatography, giving oil-like liquid as *Cl-bbt*. The yield is 70%.

Preparation of 1-(5-Chloropentyl)-1*H*-benzo[*d*][1,2,3]-triazole (*Cl-pebt*). The synthetic procedure of *Cl-pebt* is similar as that of *Cl-bbt*. K_2CO_3 (4.1 g, 0.030 mol) and 1-bromo-5-chloropentane (3.3 mL, 0.025 mol) were added to a solution of *bta* (3.0 g, 0.025 mol) in acetonitrile (100 mL). The reaction mixture was kept stirring for 2 days at room temperature. Crude product was obtained by removal of acetonitrile from filtered clear solution under reduced pressure. Then the crude product was purified by column chromatography, giving oil-like liquid as *Cl-pebt*. The yield is 67%.

Preparation of 1-(3-Chloropropyl)-5-fuloro-1*H*-benzo[*d*]-[1,2,3]triazole (*Cl-5-F-pbt*). The synthetic procedure of *Cl-5-F-pbt* is similar as that of *Cl-bbt*. *5-F-bta* (2.74 g, 0.02 mol) was dissolved in acetonitrile (100 mL), and then K_2CO_3 (3.45 g, 0.025 mol) and 1-bromo-3-chlorohexane (2.5 mL, 0.025 mol) were added to it at room temperature. The reaction mixture was kept stirring for 3 days before the solution was filtered. The filtrate was evaporated under reduced pressure, and then purified by column chromatography, giving oil-like liquid as *Cl-5-F-pbt*. The yield is 65%.

Preparation of 1-(3-Chloropropyl)-5-methyl-1*H*-benzo[*d*]-[1,2,3]triazole (*Cl-5-me-pbt*). The synthetic procedure of *Cl-5-me-pbt* is similar as that of *Cl-bbt*. 5-methyl-1*H*-benzotriazole (3.3 g, 0.025 mol) was dissolved in acetonitrile (100 mL), and then K_2CO_3 (4.1 g, 0.030 mol) and 1-bromo-3-chlorohexane (2.5 mL, 0.025 mol) were added to it at room temperature. The reaction mixture was kept stirring for 4 days before the solution was filtered. The filtrate was evaporated under reduced pressure, and then purified by column chromatography, giving oil-like liquid as *Cl-5-me-pbt*. The yield is 72%.

Preparation of 1-(3-Chloropropyl)-5,6-dimethyl-1*H*-benzo-[*d*][1,2,3]triazole (*Cl-5,6-dm-pbt*). The synthetic procedure of *Cl-5,6-dm-pbt* is similar as that of *Cl-bbt*. 5,6-Dimethyl-1*H*-benzo[*d*]-[1,2,3]triazole (3.7 g, 0.025 mol) was dissolved in acetonitrile (100 mL), K_2CO_3 (4.1 g, 0.030 mol), and 1-bromo-3-chlorohexane (2.5 mL, 0.025 mol) were added at room temperature. The reaction mixture was kept stirring for 3 days before the solution was filtered. The filtrate was evaporated under reduced pressure, then purified by column chromatography, giving white solid as *Cl-5,6-dm-pbt*. The yield is 75%.

Preparation of 1-(3-Chloro-2-methylpropyl)-1*H*-benzo[*d*]-[1,2,3]triazole (*Cl-mpbt*). The synthetic procedure of *Cl-mpbt* is similar as that of *Cl-bbt*. *Bta* (3.0 g, 0.025 mol) was dissolved in acetonitrile (100 mL), and then K_2CO_3(4.1 g, 0.030 mol) was added. 1-Bromo-3-chloro-2-methylpropane (2.9 mL, 0.025 mol) was added

https://dx.doi.org/10.1021/jacs.9b13772
J. Am. Chem. Soc. 2020, 142, 4242−4253

dropwise at room temperature. The reaction mixture was kept stirring for 2 days. Then the filtrate was evaporated under reduced pressure after the solution was filtered. The crude product was purified by column chromatography, giving oil-like liquid as *Cl-mpbt*. The yield is 55%.

Preparation of *N*-((1*H*-Benzo[*d*][1,2,3]triazol-1-yl)methyl)-*N*,*N*-dimethylethanaminium (L_1, *btdmem*) Iodide. The mixture of *Cl-mbt* (3.8 g, 0.025 mol) and KI (5 g) in acetone (20 mL) was stirred for 2 h before the solution was filtered. The filtrate was evaporated under reduced pressure then added with acetonitrile (100 mL) and *N*,*N*-dimethylethylamine (3.2 mL). After stirring at 60 °C for 2 days, a white precipitate was formed. The reaction mixture was evaporated under reduced pressure, washed with ethyl ether, and dried under a vacuum as the final product. The yield is 62%.

Preparation of *N*-((1*H*-Benzo[*d*][1,2,3]triazol-1-yl)methyl)-*N*,*N*-dimethylpropan-2-aminium (L_2, *btdmpm*) Iodide. *Cl-mbt* (3.8 g, 0.025 mol) was fully dissolved in acetone (20 mL) and KI (5 g) was added. The mixture was stirred for 2 h at room temperature before the solution was filtered. The filtrate was evaporated under reduced pressure then added with acetonitrile (100 mL) and *N*,*N*-dimethylisopropylamine (3.1 mL). The precipitate was formed after stirring under 60 °C for 3 days. The reaction mixture was evaporated under reduced pressure, washed with ethyl ether, and dried under a vacuum as the final product. The yield is 53%.

Preparation of 4-(1*H*-Benzo[*d*][1,2,3]triazol-1-yl)-*N*,*N*,*N*-trimethylbutan-1-aminium (L_3, *bttmb*) Iodide. *Cl-bbt* (5.2 g, 0.025 mol) was fully dissolved in acetone (100 mL) and KI (5 g) was added. The mixture was stirred for 2 h at room temperature before the solution was filtered. The filtrate was evaporated under reduced pressure then added with Acetonitrile (100 mL) and trimethylamine (33 wt % in ethanol solution 7.1 mL). The precipitate was formed after stirring under 60 °C for 2 days. The reaction mixture was evaporated under reduced pressure, washed with ethyl ether, and dried under a vacuum as the final product. The yield is 62%.

Preparation of 5-(1*H*-Benzo[*d*][1,2,3]triazol-1-yl)-*N*,*N*,*N*-trimethylpentan-1-aminium (L_4, *bttmpe*) Iodide. KI (5 g) was added into the solution of *Cl-pebt* (5.6 g, 0.025 mol) in acetone (100 mL). The mixture was stirred for 2 h at room temperature and then was filtered. The acetone in filtrate was evaporated under reduced pressure then acetonitrile (100 mL) and trimethylamine (33 wt % in ethanol solution 7.1 mL) were added. The crude product was formed after stirring under 60 °C for 2 days. The reaction mixture was evaporated under reduced pressure, washed with ethyl ether, and dried under a vacuum as the final product. The yield is 52%.

Preparation of 3-(5-Fluoro-1*H*-benzo[*d*][1,2,3]triazol-1-yl)-*N*,*N*,*N*-trimethylpropan-1-aminium (L_5, 5-*F*-*bttmp*) Iodide. The mixture of *Cl*-5-*F*-*pbt* (5.3 g, 0.025 mol) and KI (5 g) were added into acetone (100 mL). The mixture was stirred for 2 h before filtration. The filtrate was evaporated under reduced pressure and then dissolved in Acetonitrile (100 mL). Trimethylamine (33 wt % in ethanol solution 7.1 mL) was added before stirring under 60 °C for 3 days. After evaporating the reaction mixture under reduced pressure crude product was afforded as pale yellow solid. Washing with ethyl ether and recrystallizing with ethanol gives pure product. The yield is 80%.

Preparation of 3-(5-Methyl-1*H*-benzo[*d*][1,2,3]triazol-1-yl)-*N*,*N*,*N*-trimethylpropan-1-aminium (L_6, 5-*m*-*bttmp*) Iodide. L_6 was synthesized in a similar way as L_5. *Cl*-5-*me*-*pbt* (5.3 g, 0.025 mol) was fully dissolved in acetone (100 mL) and KI (5 g) was added. The mixture was stirred for 2 h at room temperature before the solution was filtered. The filtrate was evaporated under reduced pressure then added with acetonitrile (100 mL) and trimethylamine (33 wt % in ethanol solution 7.1 mL). The precipitate was formed after stirring under 60 °C for 2 days. The reaction mixture was evaporated under reduced pressure, washed with ethyl ether, and dried under a vacuum as the final product. The yield is 54%.

Preparation of 3-(5,6-Dimethyl-1*H*-benzo[*d*][1,2,3]triazol-1-yl)-*N*,*N*,*N*-trimethylpropan-1-aminium (L_7, 5,6-*dm*-*bttmp*) Iodide. The mixture of the solution of *Cl*-5,6-*dm*-*pbt* (5.6 g, 0.025 mol) in acetone (100 mL) and KI (5 g) stirred for 2 h at room temperature before the solution was filtered. The filtrate was evaporated under reduced pressure. The residue was dissolved in acetonitrile (100 mL) and then added with trimethylamine (33 wt % in ethanol solution 7.1 mL). The reaction mixture was stirred at 60 °C for 2 days and then evaporated under reduced pressure to afford the crude product, which was then purified by washing with ethyl ether, and dried under a vacuum as the final product. The yield is 62%.

Preparation of 3-(1*H*-Benzo[*d*][1,2,3]triazol-1-yl)-*N*,*N*,*N*,2-tetramethylpropan-1-aminium (L_8, *bttmmp*) Iodide. The mixture of the solution of *Cl-mpbt* (4.2 g, 0.025 mol) in acetone (100 mL) and KI (5 g) stirred for 2 h at room temperature before the solution was filtered. The filtrate was evaporated under reduced pressure. The residue was dissolved in acetonitrile (100 mL) and then added with trimethylamine (33 wt % in ethanol solution 7.1 mL). The reaction mixture was stirred at 60 °C for 2 days and then evaporated under reduced pressure to afford the crude product, which was then purified by washing with ethyl ether, and dried under a vacuum as the final product. The yield is 64%.

Single Crystal Growth and Pure Phase Crystalline Powder Syntheses of Compound 1−8. Single crystals of compound **1**−**8** were grown by slow diffusion method. Commercial CuI was dissolved in KI saturated solution. The ligands were dissolved in methanol. The ligands and CuI solutions were sandwiched by a layer of acetonitrile in order to prevent the direct mixing of two solutions. High quality single crystals along with pure phase crystalline powder of the hybrid structures would generally form in a few days.

Synthesis of 1D-$Cu_4I_6(L_1)_2$ (1). Acetonitrile (2 mL) was added slowly into the solution of CuI (0.038 g, 0.2 mmol) in KI saturated solution (2 mL) in a reaction vial. Then the ligand L_1 (33 mg, 0.1 mmol) in methanol (2 mL) was added slowly into the vial. Rod-shaped single crystals along with pure phase crystalline powder formed in 2 days and were collected by filtration. Yield is 64%.

Synthesis of 1D-$Cu_6I_8(L_2)_2$ (2). Solution of CuI (0.057 g, 0.3 mmol) in KI saturated solution (2 mL), acetonitrile (2 mL) and the solution of ligand L_2 (34.6 mg, 0.1 mmol) in methanol (2 mL) was added in sequence into the vial. Block-like yellow single crystals along with pure phase crystalline powder formed in 2 days and were collected by filtration. Yield is 64%.

Synthesis of 1D-$Cu_8I_{10}(L_3)_2$ (3). To a glass tube with solution of L_3 (23.3 mg, 0.1 mmol) in methanol (4 mL), CuI (0.076 g, 0.2 mmol) was added. The glass tube was kept in the 120 °C oven for 3 days after sealing. Plate-shaped single crystals formed and were collected by filtration. Yield is 54%.

Synthesis of 1D-$Cu_4I_6(L_4)_2$ (4). CuI (0.076 g, 0.2 mmol), the ligand L_4 (37.4 mg, 0.1 mmol) in methanol (4 mL) was sealed into a glass tube. The glass tube was kept in the 120 °C oven for 3 days. Block-shaped single crystals along with pure phase crystalline powder formed and were collected by filtration. Yield is 65%.

Synthesis of 1D-$Cu_4I_6(L_5)_2$ (5). To a vial with solution of CuI (0.038 g, 0.2 mmol) in KI saturated (1 mL), acetonitrile (1 mL) was added as another layer and then the solution of the ligand L_5 (36 mg, 0.1 mmol) in methanol (1 mL) was added slowly in to the vial. Plate-shaped single crystals along with pure phase crystalline powder formed in 2 days and were collected by filtration. Yield is 55%.

Synthesis of 1D-$Cu_4I_6(L_6)_2$ (6). Compound **6** was synthesized in the same way as that of **5** using CuI and L_6. Plate-shaped single crystals with pure phase crystalline powder were obtained in 2 days. Yield is 70%.

Synthesis of 1D-$Cu_4I_6(L_7)_2$ (7). Compound **7** was synthesized in the same way as that of **5**, using CuI and L_7. Rod-shaped single crystals with pure phase crystalline powder were obtained in 2 days. Yield is 65%.

Synthesis of 1D-$Cu_4I_6(L_8)_2$ (8). Compound **8** was synthesized in the same way as that of **5**, using CuI and L_8. Block-shaped single crystals with pure phase crystalline powder were obtained in 2 days. Yield is 60%.

Solubility Experiments. All solubility measurements were done under room temperature. 50 mg of pregrinded fine powder sample was first put into a clean glass vial, DMSO was then added dropwise under sonication until all solid sample dissolved and the solution

https://dx.doi.org/10.1021/jacs.9b13772
J. Am. Chem. Soc. 2020, 142, 4242−4253

became clear. The amount of DMSO added was recorded and used to calculate the solubility.

Film Fabrication. Precursor solutions of Compounds **2** and **6** (0.15 M) in DMSO were made and filtered using PTFE filter (0.45 μm) before use. High quality thin films were fabricated by one-step spin coating (WS-650Mz-23NPPB Spin Processor, Laurell Technologies) of 75 μL precursor solution onto precleaned glass substrates at 3000 rpm for 60 s, followed by annealing at 110 °C for 30 min.

Single Crystal X-ray Diffraction (SCXRD). Single crystal data of **1**−**8** were collected on a D8 goniostat equipped with a Bruker PHOTON100 CMOS detector at the Advanced Light Source (ALS), Lawrence Berkeley National Laboratory, using synchrotron radiation. The structures were solved by direct methods and refined by full-matrix least-squares on F^2 using the Bruker SHELXTL package. These data can be obtained free of charge from The Cambridge Crystallographic Data Centre via www.ccdc.cam.ac.uk/data_request/cif. The structures were deposited in Cambridge Crystallographic Data Centre (CCDC) with numbers 1943652−194655, 1946658−1943661.

Powder X-ray Diffraction (PXRD) Analysis. Powder X-ray diffraction (PXRD) analyses were carried out on a Rigaku Ultima-IV unit using Cu Kα radiation (λ = 1.5406 Å). The data were collected at room temperature in a 2θ range of 3−40° with a scan speed of 2°/min. The operating power was 40 kV/40 mA.

Room-Temperature Photoluminescence Measurements. Photoluminescence (PL) measurements were carried out on a Horiba Duetta fluorescence spectrophotometer. Powder samples were evenly distributed and sandwiched between two glass slides (which do not have emission in the visible range) for room temperature measurements.

Temperature-Dependent Photoluminescence Spectra and Lifetime Measurements. Pressed pellets were prepared in a 10 mm diameter die with the pressure of approximately 2000 psi. Temperature dependent photoluminescence (PL) spectra and time-resolved PL decays were recorded with a home-built time-correlated single photon counting instrument consisting of a 380 nm frequency doubled femtosecond solid state laser system laser as optical excitation source (frequency doubled Titanium sapphire laser, Maitai-Spectra Physics, 100 fs pulse, 10 kHz repetition rate), a Janis cryostat model V500, and an optical detection system comprised of a single photon counting avalanche photodiode (PMD50, Picoquant Germany, 250 ps response time), a time analyzer (TimeHarp 260 nano, Picoquant Germany) and an Ocean Optics FL65000 fiber optics spectrometer. The PL signal emitted by the sample was collected by a 50 mm biconvex lens and split by a 50/50 non polarizing beam splitter cube between the photodiode and spectrometer. PL signals were acquired using an average power of 0.55 mW, with decays recorded in at least 1000 channels using a 532 nm long-pass filter (Semrock). PL decays were individually fit with the Fluofit Picoquant software using a biexponent fit model.

Thermogravimetric Analysis. Thermogravimetric analyses (TGA) of samples were performed using the TA Instrument Q5000IR thermal gravimetric analyzer with nitrogen flow and sample purge rate at 10 and 12 mL/min, respectively. About 3 mg of samples were loaded onto a platinum sample pan and heated from room temperature to 450 °C at a rate of 10 °C/min under nitrogen flow.

Diffuse Reflectance Spectroscopy. Optical absorption spectra were measured at room temperature on a Shimadzu UV-3600 UV−vis−NIR spectrometer. The reflectance data were converted to Kubelka−Munk function, $\alpha/S = (1 - R)^2/2R$ (α is absorption coefficient, S is scattering coefficient and R is reflectance), and used to estimate the bandgap. The scattering coefficient (S) was treated as a constant as the average particle size of the samples used in the measurements was significantly larger than 5 μm. Samples for reflectance measurements were prepared by evenly distributing ground powder sample between two quartz slides.

Infrared Spectroscopy. IR measurements were performed on a Nicolet 6700 FTIR spectrometer equipped with a liquid N_2-cooled mercury cadmium telluride MCT-A detector. The sample of compound (~2 mg) was pressed onto a KBr pellet and placed into a vacuum cell placed at the focal point of the sample compartment of the infrared spectrometer. The cell was connected to a vacuum line for evacuation. All spectra were recorded under a vacuum (base pressure <20 mTorr) in transmission mode with a frequency range of 600−4000 cm^{-1} (4 cm^{-1} spectral resolution).

DFT Calculations. Electronic bandgaps and density of states (DOS) were calculated using Cambridge Serial Total Energy Package (CASTEP) in Materials studio.[16,23−25] Binding energies and vibrational modes were calculated using VASP.[26−31] The pK_a and pK_b values of ligands were calculated using (B3LYP/6-31+G(d)) as implemented in Gaussian 16.[32,33] The HOMO and LUMO energies of ligands were calculated using Gaussian 09 with B3LYP/6-31+G(d) basis set.[34] All the calculation details can be found in Supporting Information, sections S5 and S6.

Internal Quantum Yield (IQY) Measurements. IQY measurements were made on C9920−02 absolute quantum yield measurement system (Hamamatsu Photonics) with 150 W xenon monochromatic light source and 3.3 in. integrating sphere. Samples for internal quantum yield measurements were prepared by spreading fine powder samples evenly on the bottom of a quartz sample holder. Sodium salicylate (SS) and YAG:Ce^{3+} were chosen as the standards with reported IQY values of 60% and 95% at an excitation energy of 360 and 450 nm, respectively. Their IQY values were measured to be 63% and 97%, respectively, and corrections were made based on the reported data.

RESULTS AND DISCUSSION

Structure Design and Description. All 1D-AIO structures contain one-dimensional anionic $Cu_mI_{m+2}^{2-}$ chains and benzotriazole-based cationic ligands. The inorganic and organic modules are further connected by Cu−N coordinate bonds. The ionic bonds in these structures enhance their solubility and framework stability while the coordination bonds play a key role in their MLCT emission process. To construct such hybrid structures, cationic organic ligands of desired LUMO energies with free and strong binding sites were designed and synthesized. The cationic nature of the ligands will ensure the formation of ionic compounds with anionic inorganic modules, while the free binding sites enable the direct and strong coordination of N to Cu.

The molecular structures of organic ligands (L_1−L_8) are shown in Figure 1a. These structures were confirmed by ^{1}H NMR analysis (Figures S1−S8). All are benzotriazole derivatives with different substitute groups. They were obtained by alkylation of selected tertiary amines with substituted benzotriazole derivatives. Each ligand (L_1 through L_8) leads to the formation of a 1D-AIO structure, namely, 1D-$Cu_4I_6(L_1)_2$, 1D-$Cu_6I_8(L_2)_2$, 1D-$Cu_8I_{10}(L_3)_2$, 1D-$Cu_4I_6(L_4)_2$, 1D-$Cu_4I_6(L_5)_2$, 1D-$Cu_4I_6(L_6)_2$, 1D-$Cu_4I_6(L_7)_2$, and $Cu_4I_6(L_8)_2$. Detailed procedures for the synthesis of ligands and corresponding hybrid compounds are described in the Experimental Section. Generally, slow diffusion of CuI in saturated KI aqueous solution, acetonitrile and ligand in methanol solution at room temperature led to high quality single crystals. Selected single crystal images are displayed in Figures S12. Their crystal structures were determined by SCXRD method, and important crystallographic data are summarized in Table 1. The phase purity of the powder samples was confirmed by PXRD analysis (Figures S13 and S14).

Four types of $Cu_mI_{m+2}^{2-}$ anionic chains are obtained for the 1D-AIO structures, namely, 1D-$Cu_4I_6^{2-}$ (type-1, compound **1**), 1D-$Cu_4I_6^{2-}$ (type-2, compounds **4**−**8**), 1D-$Cu_6I_8^{2-}$ (compound **2**), and 1D-$Cu_8I_{10}^{2-}$ (compound **3**), as depicted in Figure 1b and Figure S11. Within anionic inorganic chains,

https://dx.doi.org/10.1021/jacs.9b13772
J. Am. Chem. Soc. 2020, 142, 4242−4253

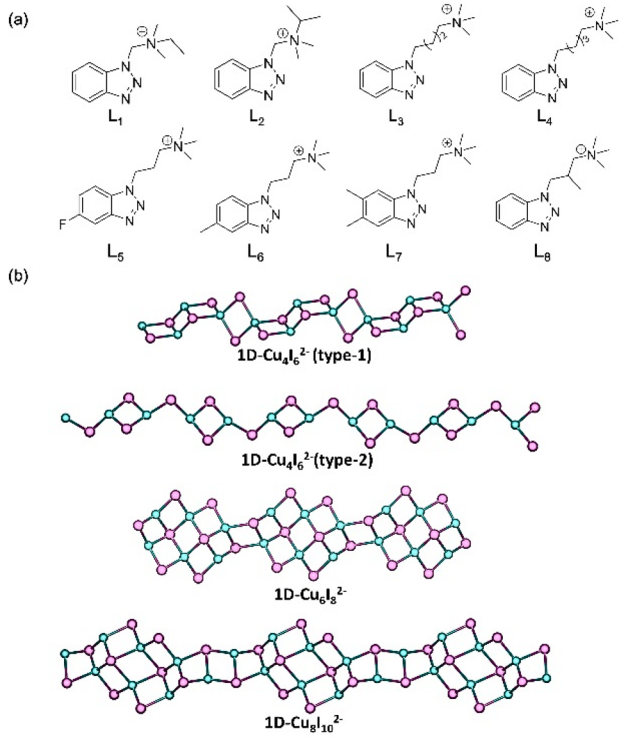

Figure 1. (a) Structures of ligands (L_1–L_8). (b) Structures of four types of inorganic chains. Color scheme: Cu, cyan; I, purple.

all copper atoms are tetrahedrally coordinated to either four iodine atoms, or three iodine atoms and one ligand. All tetrahedra are edge-sharing. The coordination number of iodine atoms varies from 2 to 4. Some anionic chains have the same composition but different structure. For example, 1D-$Cu_4I_6^{2-}$ has two types of structures (type-1 and type-2), as illustrated in Figure 1b. All anionic chains are coordinated to cationic ligands via Cu–N coordination bonds so that the overall hybrid structures are charge neutral. The Cu–N distances in these compounds are similar to typical Cu–N bond lengths found in other CuI-based hybrid structures composed of Cu–N coordinate bonds only, ~2.0–2.2 Å. As mentioned earlier, there are two N atoms in each ligand molecule that are available as free binding sites to form Cu–N bonds, which gives rise to two different coordination modes. The title structures can be classified into two subgroups based on these two coordination modes (see Figure S9, S10).

In the first subgroup, only one N atom in each ligand molecule is coordinated to the copper iodide chain via a monocoordination (μ^1-MC) mode. Two anionic chains, 1D-$Cu_4I_6^{2-}$ (type-1) and 1D-$Cu_6I_8^{2-}$, adopt this mode, forming compounds **1, 2**. For the second subgroup, two N atoms of each ligand molecule are involved in Cu–N bonding via a dicoordination (μ^2-DC) mode, forming a five-member ring with two Cu atoms and a bridging I (Figure 2). Two remaining anionic chains, namely, 1D-$Cu_4I_6^{2-}$ (type-2) and 1D-$Cu_8I_{10}^{2-}$ adopt this mode, leading to compounds **3**–**8**. The main reason for the two different coordination modes may be attributed to the length of the alkyl chain of the organic ligands. When the alkyl chain between the benzotriazole and ammonium is too short, the electron density of the middle nitrogen atom (N1) is reduced substantially due to the inductive effect,[35] thus resulting in a μ^1-MC structure in which there is no coordinate bond between N1 and Cu atom. Such an effect is negligible for

Table 1. Crystal Data of Compounds 1–8

compound	1D-$Cu_4I_6(L_1)_2$ (1)	1D-$Cu_6I_8(L_2)_2$ (2)	1D-$Cu_8I_{10}(L_3)_2$ (3)	1D-$Cu_4I_6(L_4)_2$ (4)	1D-$Cu_4I_6(L_5)_2$ (5)	1D-$Cu_4I_6(L_6)_2$ (6)	1D-$Cu_4I_6(L_7)_2$ (7)	1D-$Cu_4I_6(L_8)_2$ (8)
ligand abbreviation	*btdmem*	*btdmpm*	*bttmb*	*bttmpe*	*5-F-bttmp*	*5-m-bttmp*	*5,6-dm-bttmp*	*bttmmp*
coordination mode	μ^1-MC		μ^2-DC					
empirical formula	$C_{11}H_{17}Cu_2I_3N_4$	$C_{12}H_{19}Cu_3I_4N_4$	$C_{13}H_{21}Cu_4I_5N_4$	$C1_4H_{23}Cu_2I_3N_4$	$C_{12}H_{18}Cu_2FI_3N_4$	$C_{13}H_{21}Cu_2I_3N_4$	$C_{14}H_{23}Cu_2I_3N_4$	$C_{13}H_{21}Cu_2I_3N_4$
FW	713.07	917.53	1122.00	755.14	745.08	741.12	755.14	741.12
space group	$P2_1/c$	$P2_1/n$	$P\bar{1}$	$P\bar{1}$	$P2_1/n$	$P2_1/n$	$P2_1/n$	$P2_1/n$
a (Å)	10.4474(4)	9.8380(5)	10.0745(4)	9.3391(5)	10.8072(8)	10.6544(4)	10.5764(4)	9.4891(4)
b (Å)	10.2493(4)	17.9705(9)	10.3622(4)	11.1574(6)	15.8476(12)	16.2530(7)	17.2108(6)	12.6947(5)
c (Å)	16.7427(6)	12.5124(7)	13.8122(5)	11.4854(6)	12.2010(9)	12.0841(5)	11.6786(4)	16.4418(6)
α (deg)	90	90	103.484(2)	93.313(3)	90	90	90	90
β (deg)	104.1650(10)	108.977(2)	103.345(2)	110.774(3)	109.491(3)	107.326(2)	106.7980(10)	94.924(2)
γ (deg)	90	90	110.523(2)	107.758(3)	90	90	90	90
V (Å^3)	1738.27(11)	2091.88(19)	1233.41(8)	1046.98(10)	1969.9(3)	1997.61(14)	2035.12(13)	1973.29(13)
Z	4	4	2	2	4	4	4	4
T (K)	100(2)	100(2)	100(2)	100(2)	100(2)	100(2)	100(2)	100(2)
λ (Å)	0.7293	0.7749	0.7288	0.7749	0.7288	0.7288	0.7288	0.72880
R_1	0.0184	0.0200	0.0261	0.0249	0.0330	0.0356	0.0301	0.0217
wR_2	0.0435	0.0454	0.0657	0.0497	0.0792	0.0761	0.0669	0.0488

https://dx.doi.org/10.1021/jacs.9b13772
J. Am. Chem. Soc. 2020, 142, 4242–4253

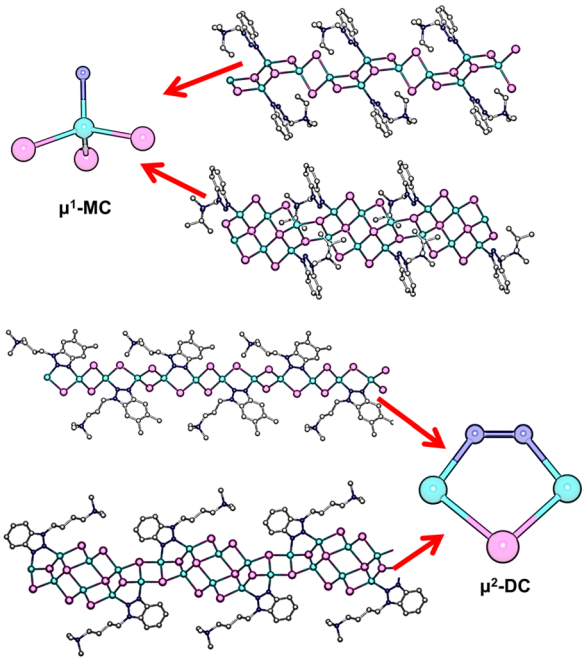

Figure 2. Illustration of μ^1-MC and μ^2-DC mode and representative hybrid structures. Color scheme: Cu, cyan; I, purple; N, blue; C, Gray.

longer alkyl chains, therefore, both N atoms (N1 and N2) form bonds to the two adjacent Cu atoms to give μ^2-DC structures. This is confirmed by the pK_b values calculated for different N atoms in each ligand. As shown in Figure 3 and Table S6, for

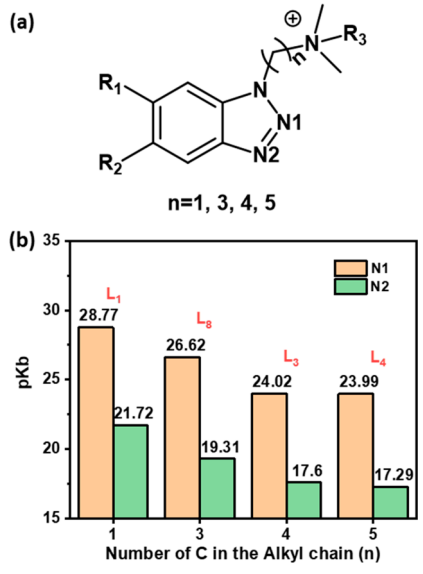

Figure 3. (a) Ligand structures used to calculate pK_b values of N1 and N2. (b) pK_b values of N1 and N2 in selected ligands of different alkyl chain length (n = number of C atoms in alkyl linear chain).

all ligands, the pK_b values are generally larger for N1 than N2, and are the largest for N1 of L_1 and L_2. The very weak Lewis basicity of these N1 atoms prevents the formation of Cu−N1 bonds, resulting in μ^1-MC structures (see SI for calculation details). In addition, the two adjacent Cu atoms that are available to form 5-member rings are too far apart in the μ^1-MC structures (~4.16 Å for both **1** and **2**, see Table S1).

Photophysical Properties. The photophysical properties of the 1D-AIO hybrids at room temperature were characterized using UV−vis absorption spectroscopy, as well as photoluminescence emission spectroscopy. The important photophysical properties of these hybrid structures are summarized in Table 2. The optical absorption spectra are given in Figures S17 and S18. The high absorption coefficients suggest that they are strong energy absorbers, which are ideal for phosphors. Their bandgaps were estimated from optical absorption data and the values are listed in Table 2. All compounds emit low energy colors between green and red (528 to 650 nm), and all can be excited by blue light, an important requirement for phosphors that can be used in conjunction with a blue LED chip as in the current commercial WLED devices. Room temperature solid state photoluminescence experiments confirm that the emission profile of all compounds is a single band type with a full width at half-maximum (fwhm) around 100 nm, similar to those observed for commercial phosphors (Figure 4a, Figures S19, S20).[36,37]

The PL lifetime measurements were carried out at 77 to 293 K on selected 1D-AIO compounds from both subgroups (see Figures S21−S24). All of them exhibit strong temperature dependence, as their average amplitude-weighted lifetime values decrease from ~16 μs at 77 K to ~2 μs at 293 K (Tables S2−S5). The PL lifetime decay curves are best fit by a double (second order) exponential decay function, indicating two different processes contribute to their emission. Using compound **7** as an example, the fraction of the short lifetime decay constant τ_1 rises from 39.25% at 77 K to 69.96% at 293 K. These data suggest that besides phosphorescence, thermally activated delayed fluorescence (TADF) also contributes largely to the emission of 1D-AIO structures. Due to small energy differences between the lowest excited singlet state (S_1) and the triplet state (T_1), a fraction of electrons can undergo reverse intersystem crossing (RISC) from T_1 back to S_1, and then follow a radiative transition from S_1 to S_0. This phenomenon has been observed in a number of copper-based organic−inorganic hybrid materials.[16,38−40] The emission mechanism of 1D-AIO can be considered as a combination of both TADF and phosphorescence.

Although the emission energies and PL mechanism are similar for μ^1-MC and μ^2-DC structures, their emission intensity and IQYs differ significantly. The μ^2-DC structures exhibit much higher IQYs compared to those of μ^1-MC structures. As shown in Table 2, the IQYs for μ^2-DC structures are typically twice as those of μ^1-MC structures. The big variation in their emission efficiency is largely due to the difference in their coordination modes. As expected, our ab initio calculations found the μ^2-DC ligand binding to be much stronger than the μ^1-MC binding with a 150% increase in binding strength. Furthermore, a vibrational mode analysis shows that the μ^2-DC ligand−metal bond is stiffer since the stretching mode occurs at a higher frequency (Table S8). In all μ^2-DC structures, the rigid 5-member ring can effectively reduce the extent of nonradiative decay due to severely limited ligand rotation and vibration. To confirm this, we have calculated vibrational motions of C−C, C−N, stretching and C−H bending modes in compounds **1** and **3** and collected their vibrational spectra by infrared (IR) spectroscopy. Figure S29 shows that compound **1** has higher intensity IR peaks than compound **3**, likely the result of less vibrational motion in compound **3** compared to compound **1**. To quantitatively assess the degree of nonradiative decay in μ^1-MC and μ^2-DC

https://dx.doi.org/10.1021/jacs.9b13772
J. Am. Chem. Soc. 2020, 142, 4242−4253

Table 2. Important Optical and Stability Data for Compounds 1−8[a]

#	formula	band gap (eV)	λ_{em} (nm)	emission color	IQY (%) λ_{ex} = 360 nm	IQY (%) λ_{ex} = 450 nm	k_r ($\times 10^5$, s^{-1})	k_{nr} ($\times 10^5$, s^{-1})	T_D (°C)
μ^1-MC Structures									
1	1D-$Cu_4I_6(L_1)_2$	2.6	550	green-yellow	25	21	–	–	190
2	1D-$Cu_6I_8(L_2)_2$	2.5	650	red	29	24	1.42	3.48	193
μ^2-DC Structures									
3	1D-$Cu_8I_{10}(L_3)_2$	2.65	528	green	80	64	2.56	0.64	245
4	1D-$Cu_4I_6(L_4)_2$	2.45	552	green-yellow	70	64	–	–	235
5	1D-$Cu_4I_6(L_5)_2$	2.2	615	orange-red	53	44	1.88	1.67	225
6	1D-$Cu_4I_6(L_6)_2$	2.45	596	orange-red	85	76	3.78	0.67	225
7	1D-$Cu_4I_6(L_7)_2$	2.5	570	yellow-orange	68	65	4.93	2.32	235
8	1D-$Cu_4I_6(L_8)_2$	2.4	553	green-yellow	53	40	–	–	211

[a]Note: k_r = Radiative decay rate; k_{nr} = Nonradiative decay rate.

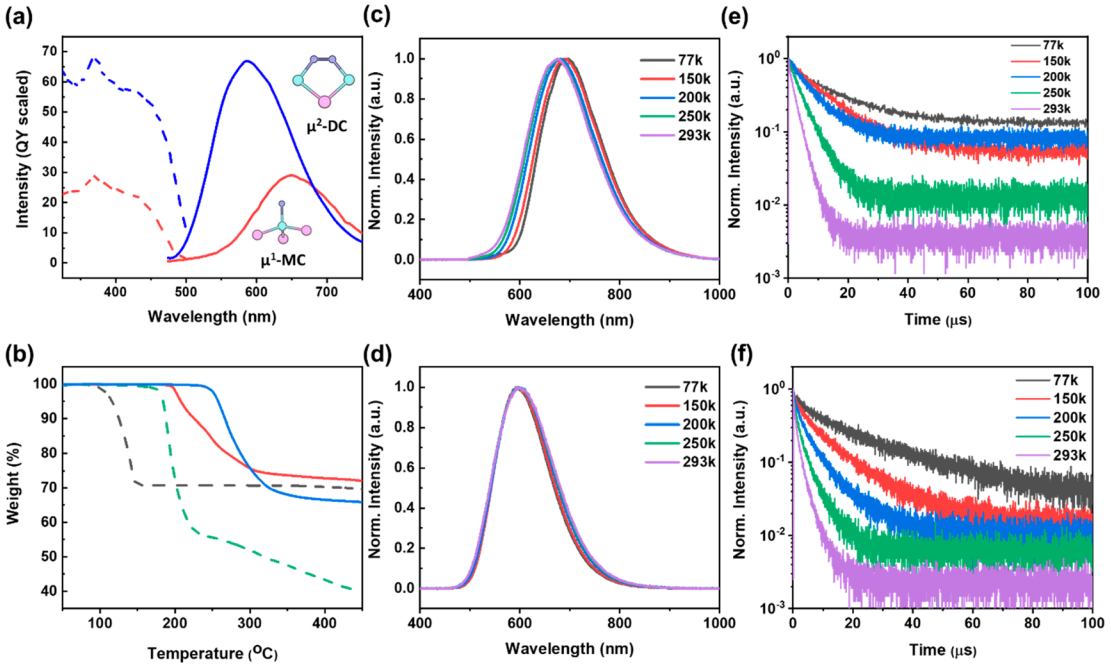

Figure 4. (a) IQY scaled emission spectra (solid) and excitation spectra (dotted) of **2** (red) and **7** (blue). (b) TGA plots of 1D-CuI(*py*) staircase chain (dotted black),[7] 0D-$Cu_4I_6(tpp)_2(bttmm)_2$[16] (dotted green), compound **2** (red) and compound **7** (blue). (c,d) Normalized emission spectra of compounds **2** and **7** at various temperatures (λ_{ex} = 380 nm). (e,f) Luminescence decay profiles of compounds **2** and **7** at various temperatures (λ_{ex} = 380 nm).

Table 3. Estimated Total Radiative and Nonradiative Decay Rates Calculated from Experimental IQY and τ_{PL} for Selected Compounds at 293 K

#	formula	τ_{PL} (μs)	τ_1 (μs)	τ_2 (μs)	A_1 (%)	A_2 (%)	k_r ($\times 10^5$, s^{-1})	k_{nr} ($\times 10^5$, s^{-1})
μ^1-MC Structures								
2	1D-$Cu_6I_8(L_2)_2$	2.04	2.48	0.64	75.79	24.21	1.42	3.48
μ^2-DC Structures								
3	1D-$Cu_8I_{10}(L_3)_2$	3.13	5.10	1.51	45.04	54.96	2.56	0.64
5	1D-$Cu_4I_6(L_5)_2$	2.82	3.20	1.13	81.96	18.04	1.88	1.67
6	1D-$Cu_4I_6(L_6)_2$	2.25	3.38	0.90	54.35	45.65	3.78	0.67
7	1D-$Cu_4I_6(L_7)_2$	1.38	2.92	0.71	30.04	69.96	4.93	2.32

structures, total radiative rates (k_r) and nonradiative decay rates (k_{nr}) were estimated based on eqs 1 and 2 below and PL lifetime and IQY data.

$$\eta = k_r/(k_r + k_{nr}) \quad (1)$$

$$\tau_{PL} = 1/(k_r + k_{nr}) \quad (2)$$

For a biexponential decay, $\tau_{PL} = A_1\tau_1 + A_2\tau_2$. A_1 and A_2 are the fractional amplitudes and τ_1 andτ_2 are the different lifetime components. η is the quantum yield value. The estimated total radiative and nonradiative decay rates for selected structures are summarized in Table 3. Note that the excitation wavelengths used for the IQY and PL lifetime measurements are slightly different (360 and 380 nm, respectively). Hence, the radiative decay rates are expected to be slightly

https://dx.doi.org/10.1021/jacs.9b13772
J. Am. Chem. Soc. 2020, 142, 4242−4253

overestimated and the nonradiative decay rates are slightly underestimated.

It is apparent that the total nonradiative decay rate is largest for compound **2**, a μ^1-MC structure. It is also notable that compounds **3** and **6** (μ^2-DC structures), having the smallest nonradiative rates and largest quantum yields, exhibit similar amplitudes of the short and long lifetime components. This observation suggests that compounds that exhibit similar contributions from phosphorescence and TADF may lead to more efficient luminescence (assuming the short lifetime component is primarily from TADF and the long lifetime component is primarily from phosphorescence). The rates in Table 3 are total radiative and nonradiative rates meaning that they represent contributions from the radiative components of both emission mechanisms (phosphorescence and TADF) as well as associated internal and external conversions and loss factors.

It is also interesting to note that only μ^1-MC hybrid structures show obvious thermoluminescence behavior. For compound **2**, about 20 nm red shift in its emission spectra was observed by lowering the temperature from 293 to 77 K (Figure 4c). This unusual thermosensitivity may be attributed to increased structural torsion at high temperature and decreased $\pi-\pi$ stacking between organic molecules due to increased vibrational and rotational motions at higher temperature.[41−43] It may also arise from increased RISC at higher temperature to a S_1 state slightly higher in energy than the T_1 state. In contrast, very little temperature dependence was detected in the emission spectra of the μ^2-DC hybrid structures (Figure 4d). This can be attributed to minimal change in the material structure with temperature or S_1 and T_1 states are almost indistinguishable in energy.

Electronic Band Structures. Density functional theory (DFT) calculations were conducted to calculate the density of states (DOS) of selected structures using the Cambridge Serial Total Energy Package (CASTEP) in Materials Studio[12,16,17] (Figure 5, Figures S25−S28). Compounds from both subgroups were investigated and the results show that their electronic band structures are very similar. On the basis of the density of states (DOS) analysis, for both types of compounds, the atomic states that make up the conduction band minimum (CBM) are mostly from organic ligands (C 2p and N 2p), while the atomic states in the valence band maximum (VBM) region are mainly from the inorganic components (Cu 3d and I 5p). These results suggest a combination of metal-to-ligand charge transfer (MLCT) and halide-to-ligand charge transfer (XLCT) luminescence mechanisms for both types of compounds, while the emission of rare-earth element containing commercial phosphors originate from the atomic orbitals of Ce^{3+} or Eu^{3+}.[36,37] Therefore, the emission wavelength of the hybrid structures is much more tunable and can be systematically regulated by using ligands with different lowest unoccupied molecular orbital (LUMO) energies (see Table S7). By adding electron withdrawing group (EWG) or electron donating group (EDG), the emission energies of compounds **5**−**8**, which differ only by a functional group in their ligand, can be tuned from 553 to 615 nm (see Figure S20).

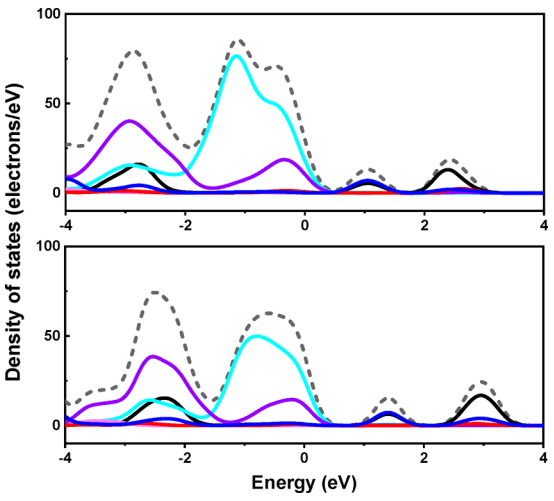

Figure 5. Density of states (DOS) and projected density of states (PDOS) plots for compound **2** (top) and compound **7** (bottom). Line color scheme: dashed black: total; cyan: Cu (3d); pink: Cu (4s); red: I (5s); purple: I (5p); black: C (2p); blue: N (2p).

Thermal Stability. The greatly enhanced thermal stability of the 1D-AIO structures is reflected from thermogravimetric (TG) analysis results. The decomposition temperatures (T_D) of these compounds are summarized in Table 2. These structures remain stable up to at least 190 °C with some reaching 245 °C (Figures S15 and S16), which are notably higher than 0D-AIO structures.[16] In general, the μ^2-DC structures are more robust than the μ^1-MC structures which can also be attributed to the difference in their coordination mode. The trend of thermal stability of compounds **4**−**8**, which share the same inorganic chain 1D-$Cu_4I_6^{2-}$ (type 2), also agrees with the calculated pK_b values (see Table S6). Smaller pK_b values of the N atoms indicate higher Lewis basicity and electron density, and stronger Cu−N bonds, leading to higher decomposition temperature. Compared to charge-neutral 1D-CuI(L) staircase chain based structures which generally decompose below 100 °C (Figure 4b), the stability of both μ^1-MC and μ^2-DC compounds is significantly enhanced, as a result of forming both ionic and coordination bonds between the inorganic chain and organic ligand.

Solubility, Solution Processability, and Thin-Film Fabrication. As stated above, one of the major obstacles for crystalline materials having covalent/coordinate network structures is their insolubility, which makes it difficult for low-cost and large-scale manufacture process. With ionic bonds introduced to the 1D copper iodide based coordinate structures, we demonstrate here that outstanding solubility in polar aprotic solvents such as DMSO can be achieved for all title compounds.

All hybrid network structures based on charge-neutral Cu_mI_m reported to date are known to be insoluble, either in organic or inorganic solvents. For example, the 1D-CuI(L) staircase chain compounds are composed of 1D-CuI inorganic module similar to those in the 1D-AIO structures. All Cu atoms are coordinated to N atoms via dative bonds in both structures. The only difference is that both inorganic chain and organic ligand are *charge-neutral* in 1D-CuI(L) staircase chain structures, while both components are *ionic* in 1D-$Cu_mI_{m+2}(L)_2$ AIO structures (Scheme 1).[7] All 1D-CuI(L) staircase chain structures, as well as all other 2D- and 3D-CuI(L) hybrid structures show very poor solubility in any common organic and inorganic solvents, including polar aprotic solvents. Taking 1D-CuI(py)[7] and 1D-Cu_4I_4(bbtpe)$_2$[12] as examples, they are barely soluble in DMSO (Figure 6b). Similarly, the 2D-Cu_2I_2(2,5-dmpz) made of 1D CuI stair-case chains and

https://dx.doi.org/10.1021/jacs.9b13772
J. Am. Chem. Soc. 2020, 142, 4242−4253

Scheme 1. Structure Similarity and Solubility Difference of Charge-Neutral 1D-CuI(L) (Left, Insoluble) and 1D-AIO-$Cu_mI_{m+2}(L)_2$ (Right, Soluble) Compounds

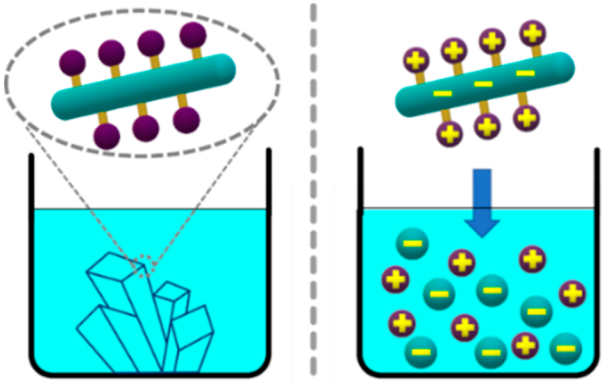

bridging ligands[44] and 3D-$Cu_4I_4(en)_2$ built on 4-connected Cu_4I_4 clusters and 2-connected ligands[8] show negligible solubility in DMSO (Table 4). In contrary, all 1D-AIO compounds exhibit remarkably high solubility in DMSO and other polar aprotic solvents, comparable with those of common ionic salts[45] (see Figure 6b and Table 4), outperformed the current commercial phosphors.

For example, about 350 mg of sample **2** can be completely dissolved in 1 mL DMSO within 5 min at room temperature under ultrasonication. Upon dissolution, it lost luminescence completely (Figure 6b). The same behavior was observed for all other 1D-AIO-$Cu_mI_{m+2}(L)_2$ compounds. All compounds can be recovered/recrystallized from the solution either by adding antisolvent such as methanol or by slowly cooling the saturated DMSO solution (preheated to 60 °C) to room temperature. It is interesting to note that their dissolution behavior may be similar to that of hybrid perovskite structures. The strong interaction between DMSO and both PbI_2[46,47] and CuI[48] have been reported. In DMSO solution of hybrid perovskite, with the presence of excess iodide ions provided by MAI, soluble PbI_3^-, PbI_4^{2-} and higher coordinated plumbate species are generated from PbI_2 complexation[49,50] and then form a trinuclear plumbate $(MA^+)_2[(PbI_3^-)_2PbI_2]\cdot(DMSO)_2$,[51] increasing the solubility of perovskites over PbI_2. Similarly, all title 1D-AIO compounds demonstrate much higher solubility in DMSO compared to CuI, possibly attributed to the formation of CuI-L-DMSO complexes as suggested by NMR analysis. While the soluble trinuclear clusters of the lead-based hybrid perovskites remain emissive in the solution, the emission is lost completely for the solution phase of 1D-AIO hybrid structures, likely due to the dissociation of Cu−N bonds, which eliminates the MLCT and XLCT charge transfer in these compounds.

High quality thin films can be prepared by directly drop-casting or spin-coating of the 1D-AIO/DMSO solutions. As shown in Figure 6d, film samples of compounds **2** and **6** were prepared by one-step spin coating of each compound dissolved in DMSO. Both luminescence and crystallinity of the film samples were restored after annealing at 110 °C (Figure 6d). The film sample of compound **6** was analyzed by atomic force microscopy (AFM) with tapping mode. The results show that

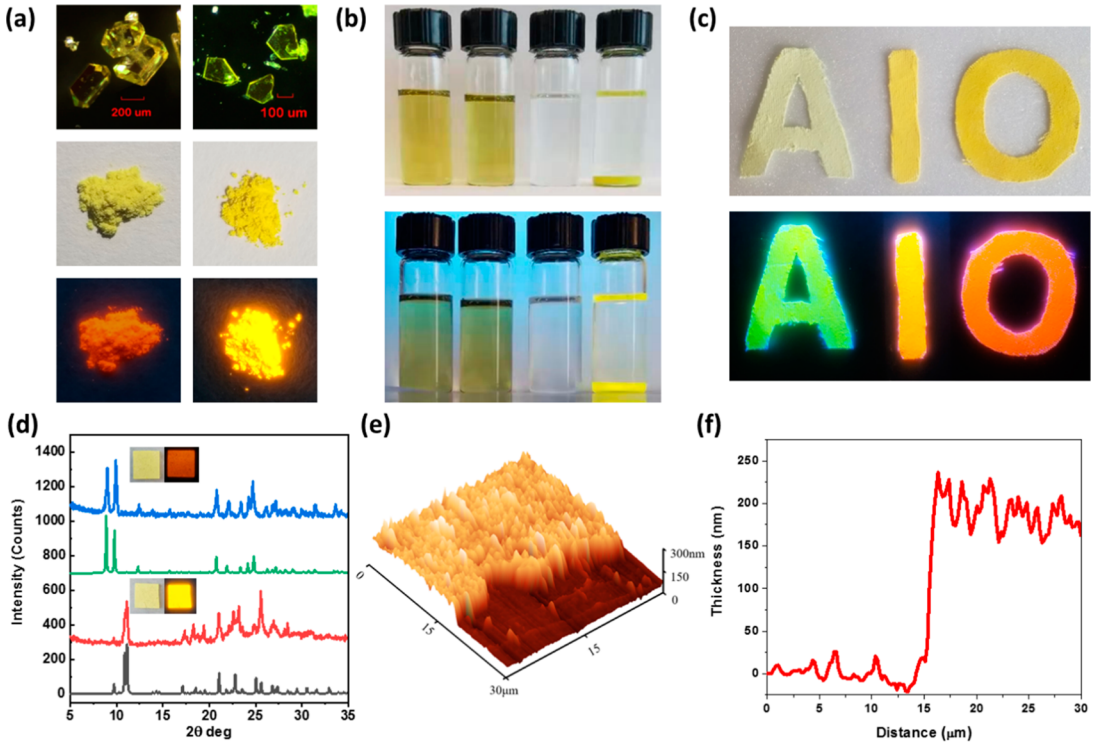

Figure 6. (a) Optical images of compounds **2** (left column) and **6** (right column). From top to bottom: crystal image under day light; Image of powder samples under day light; Image of powder samples under 365 nm UV light. (b) Optical image of 200 mg of selected compounds dissolved in 3 mL DMSO under daylight (top) and 365 nm UV light (bottom). From left to right: Compounds **2**, **6**, $PbCl_2$, and 1D-Cu_4I_4(bbtpe)$_2$ (bbtpe = 1,5-bis(1*H*-benzo[*d*][1,2,3]triazol-1-yl)pentane). (c) Selected 1D-AIO samples coated on soft fabric: under daylight (top) and 365 nm UV light (bottom). (d) PXRD patterns of thin films. From bottom to top: simulated **6**, film of **6**, simulated **2**, film of **2**. Inset: optical images of thin film samples under daylight (left) and 365 nm UV light (right). (e) AFM image and (f) sample thickness profile of a thin film of compound **6**.

https://dx.doi.org/10.1021/jacs.9b13772
J. Am. Chem. Soc. 2020, 142, 4242−4253

Table 4. Solubility Data for Compounds 1−8, Common Inorganic Salts, and Non-AIO CuI(*L*) Extended Network Structures[a]

compound	formula	solubility in DMSO (mg/mL@25 °C)	ref.
μ^1-MC 1D-AIO Structures			
1	$Cu_4I_6(L_1)_2$	210	this work
2	$Cu_6I_8(L_2)_2$	350	
μ^2-DC 1D-AIO Structures			
3	$Cu_8I_{10}(L_3)_2$	90	this work
4	$Cu_4I_6(L_4)_2$	80	
5	$Cu_4I_6(L_5)_2$	140	
6	$Cu_4I_6(L_6)_2$	80	
7	$Cu_4I_6(L_7)_2$	70	
8	$Cu_4I_6(L_8)_2$	90	
Common Inorganic Salts			
calcium nitrate	$Ca(NO_3)_2$	300	45
cuprous iodide	CuI	10 @ 30 °C	
lead chloride	$PbCl_2$	100	
lead nitrate	$Pb(NO_3)_2$	200	
lithium nitrate	$LiNO_3$	100	
potassium nitrate	KNO_3	120	
sodium nitrate	$NaNO_3$	200	
Non-AIO CuI(L) Extended Network Structures			
1D-CuI(py)	–	<10	7
1D-CuI(3-pc)	–	<10	7
1D-Cu_4I_4(bbtpe)$_2$	–	insoluble	12
2D-Cu_2I_2(2,5-dmpz)	–	insoluble	44
2D-Cu_4I_4(bpp)$_2$	–	insoluble	6
3D-Cu_4I_4(en)$_2$	–	insoluble	6

[a]py = pyridine; 3-pc = 3-picoline; bbtpe = 1,5-bis(1*H*-benzo[*d*]-[1,2,3]triazol-1-yl)pentane; 2,5-dmpz = 2,5-dimethylpyrazines; bpp = 1,3-bis(4-pyridyl)propane); en = ethylenediamine.

a continuous film with a thickness of ∼200 nm was achieved. (Figure 6e,f). This remarkably high solution processability can greatly simplify the device fabrication process currently used for REE based commercial phosphors.

CONCLUSION

In summary, we have designed and synthesized a series of 1D-AIO type of inorganic−organic hybrid structures composed of $Cu_mI_{m+2}^{2-}$ anionic 1D chains and cationic ligands of benzotriazole derivatives. These structures can be divided into two subgroups based on their coordination modes. Both subgroups show high resistance to heat and moisture, and exhibit remarkably high solubility as well as solution processability as a result of incorporation of ionic and coordinate bonds at the interface of organic and inorganic modules. High quality thin films were fabricated directly by drop-casting or spin-coating and characterized by AFM. All compounds show strong blue-light excitability, and compounds having μ^2-DC mode exhibit significant reduction of non-radiative luminescence decay, as a result of forming more rigid bonds between the inorganic and organic components, which limits vibrational motions of the ligands, thereby leading to greatly enhanced photoluminescence and a record-high IQY for blue light excited yellow-orange emission. The AIO approach may serve as a general and powerful tool for the design of high performance and easily solution processable hybrid materials including but not limited to copper halide based systems that bring promise to low-cost and large-scale device fabrication for energy-related applications.

ASSOCIATED CONTENT

Supporting Information

The Supporting Information is available free of charge at https://pubs.acs.org/doi/10.1021/jacs.9b13772.

Crystallographic data, PXRD patterns, TGA data, PL spectra, and DFT calculation results (PDF)

Crystal data (ZIP)

AUTHOR INFORMATION

Corresponding Author

Jing Li − *Department of Chemistry and Chemical Biology, Rutgers University, Piscataway, New Jersey 08854, United States; Hoffmann Institute of Advanced Materials, Shenzhen Polytechnic, Shenzhen 518055, China;* orcid.org/0000-0001-7792-4322; Email: jingli@rutgers.edu

Authors

Xiuze Hei − *Department of Chemistry and Chemical Biology, Rutgers University, Piscataway, New Jersey 08854, United States*

Wei Liu − *Hoffmann Institute of Advanced Materials, Shenzhen Polytechnic, Shenzhen 518055, China; Department of Chemistry and Chemical Biology, Rutgers University, Piscataway, New Jersey 08854, United States*

Kun Zhu − *Department of Chemistry and Chemical Biology, Rutgers University, Piscataway, New Jersey 08854, United States;* orcid.org/0000-0001-9059-513X

Simon J. Teat − *Advanced Light Source, Lawrence Berkeley National Laboratory, Berkeley, California 94720, United States*

Stephanie Jensen − *Department of Physics and Center for Functional Materials, Wake Forest University, Winston-Salem, North Carolina 27109, United States*

Mingxing Li − *Center for Functional Nanomaterials, Brookhaven National Laboratory, Upton, New York 11973, United States*

Deirdre M. O'Carroll − *Department of Chemistry and Chemical Biology and Department of Materials Science and Engineering, Rutgers University, Piscataway, New Jersey 08854, United States;* orcid.org/0000-0001-7209-4278

Kevin Wei − *Department of Materials Science & Engineering, University of Texas at Dallas, Richardson, Texas 75080, United States*

Kui Tan − *Department of Materials Science & Engineering, University of Texas at Dallas, Richardson, Texas 75080, United States;* orcid.org/0000-0002-5167-7295

Mircea Cotlet − *Center for Functional Nanomaterials, Brookhaven National Laboratory, Upton, New York 11973, United States;* orcid.org/0000-0002-5024-3540

Timo Thonhauser − *Department of Physics and Center for Functional Materials, Wake Forest University, Winston-Salem, North Carolina 27109, United States*

Complete contact information is available at: https://pubs.acs.org/10.1021/jacs.9b13772

Author Contributions

[¶]X.H. and W.L. contributed equally.

https://dx.doi.org/10.1021/jacs.9b13772
J. Am. Chem. Soc. 2020, 142, 4242−4253

Notes

The authors declare no competing financial interest.

■ ACKNOWLEDGMENTS

Financial support from the National Science Foundation (Grant No. DMR-1507210) is gratefully acknowledged. Part of the DFT calculations and infrared spectroscopic work was supported by the U.S. Department of Energy, Office of Science, Office of Basic Energy Sciences under Award DE-SC0019902. The Advanced Light Source (ALS) was supported by the Director, Office of Science, Office of Basic Energy Science, of the U.S. Department of Energy, under contract DE-AC02-05CH11231. The temperature dependent luminescence work was carried out at the Center for Functional Nanomaterials, Brookhaven National Laboratory (BNL), which is supported by the U.S. Department of Energy, Office of Basic Energy Sciences, under Contract No. DE-SC0012704.

■ REFERENCES

(1) Peng, R.; Li, M.; Li, D. Copper(I) halides: A versatile family in coordination chemistry and crystal engineering. *Coord. Chem. Rev.* **2010**, *254* (1−2), 1−18.
(2) Yam, V. W.; Au, V. K.; Leung, S. Y. Light-Emitting Self-Assembled Materials Based on d(8) and d(10) Transition Metal Complexes. *Chem. Rev.* **2015**, *115* (15), 7589−728.
(3) Tsuge, K.; Chishina, Y.; Hashiguchi, H.; Sasaki, Y.; Kato, M.; Ishizaka, S.; Kitamura, N. Luminescent copper(I) complexes with halogenido-bridged dimeric core. *Coord. Chem. Rev.* **2016**, *306*, 636−651.
(4) Perruchas, S.; Le Goff, X. F.; Maron, S.; Maurin, I.; Guillen, F.; Garcia, A.; Gacoin, T.; Boilot, J. P. Mechanochromic and thermochromic luminescence of a copper iodide cluster. *J. Am. Chem. Soc.* **2010**, *132* (32), 10967−9.
(5) Liu, Z.; Qayyum, M. F.; Wu, C.; Whited, M. T.; Djurovich, P. I.; Hodgson, K. O.; Hedman, B.; Solomon, E. I.; Thompson, M. E. A codeposition route to CuI-pyridine coordination complexes for organic light-emitting diodes. *J. Am. Chem. Soc.* **2011**, *133* (11), 3700−3.
(6) Liu, W.; Fang, Y.; Wei, G. Z.; Teat, S. J.; Xiong, K.; Hu, Z.; Lustig, W. P.; Li, J. A Family of Highly Efficient CuI-Based Lighting Phosphors Prepared by a Systematic, Bottom-up Synthetic Approach. *J. Am. Chem. Soc.* **2015**, *137* (29), 9400−8.
(7) Zhang, X.; Liu, W.; Wei, G. Z.; Banerjee, D.; Hu, Z.; Li, J. Systematic approach in designing rare-Earth-free hybrid semiconductor phosphors for general lighting applications. *J. Am. Chem. Soc.* **2014**, *136* (40), 14230−6.
(8) Fang, Y.; Liu, W.; Teat, S. J.; Dey, G.; Shen, Z. Q.; An, L. T.; Yu, D. C.; Wang, L.; O'Carroll, D. M.; Li, J. A Systematic Approach to Achieving High Performance Hybrid Lighting Phosphors with Excellent Thermal- and Photostability. *Adv. Funct. Mater.* **2017**, *27* (3), 1603444.
(9) Naik, S.; Mague, J. T.; Balakrishna, M. S. Short-bite PNP ligand-supported rare tetranuclear [Cu4I4] clusters: structural and photoluminescence studies. *Inorg. Chem.* **2014**, *53* (7), 3864−73.
(10) Volz, D.; Zink, D. M.; Bocksrocker, T.; Friedrichs, J.; Nieger, M.; Baumann, T.; Lemmer, U.; Brase, S. Molecular Construction Kit for Tuning Solubility, Stability and Luminescence Properties: Heteroleptic MePyrPHOS-Copper Iodide-Complexes and their Application in Organic Light-Emitting Diodes. *Chem. Mater.* **2013**, *25* (17), 3414−3426.
(11) Yu, M.; Chen, L.; Jiang, F.; Zhou, K.; Liu, C.; Sun, C.; Li, X.; Yang, Y.; Hong, M. Cation-Induced Strategy toward an Hourglass-Shaped Cu6I7- Cluster and Its Color-Tunable Luminescence. *Chem. Mater.* **2017**, *29* (19), 8093−8099.
(12) Fang, Y.; Sojdak, C. A.; Dey, G.; Teat, S. J.; Li, M.; Cotlet, M.; Zhu, K.; Liu, W.; Wang, L.; Dm, O. C.; Li, J. Highly efficient and very robust blue-excitable yellow phosphors built on multiple-stranded one-dimensional inorganic-organic hybrid chains. *Chem. Sci.* **2019**, *10* (20), 5363−5372.
(13) Liu, W.; Fang, Y.; Li, J. Copper Iodide Based Hybrid Phosphors for Energy-Efficient General Lighting Technologies. *Adv. Funct. Mater.* **2018**, *28* (8), 1705593.
(14) Liu, W.; Lustig, W. P.; Li, J. Luminescent inorganic-organic hybrid semiconductor materials for energy-saving lighting applications. *EnergyChem.* **2019**, *1* (2), 100008.
(15) Ford, P. C.; Cariati, E.; Bourassa, J. Photoluminescence Properties of Multinuclear Copper(I) Compounds. *Chem. Rev.* **1999**, *99* (12), 3625−3648.
(16) Liu, W.; Zhu, K.; Teat, S. J.; Dey, G.; Shen, Z.; Wang, L.; O'Carroll, D. M.; Li, J. All-in-One: Achieving Robust, Strongly Luminescent and Highly Dispersible Hybrid Materials by Combining Ionic and Coordinate Bonds in Molecular Crystals. *J. Am. Chem. Soc.* **2017**, *139* (27), 9281−9290.
(17) Chen, S.; Gao, J.; Chang, J.; Li, Y.; Huangfu, C.; Meng, H.; Wang, Y.; Xia, G.; Feng, L. Family of Highly Luminescent Pure Ionic Copper(I) Bromide Based Hybrid Materials. *ACS Appl. Mater. Interfaces* **2019**, *11* (19), 17513−17520.
(18) Zhou, C.; Tian, Y.; Yuan, Z.; Lin, H.; Chen, B.; Clark, R.; Dilbeck, T.; Zhou, Y.; Hurley, J.; Neu, J.; Besara, T.; Siegrist, T.; Djurovich, P.; Ma, B. Highly Efficient Broadband Yellow Phosphor Based on Zero-Dimensional Tin Mixed-Halide Perovskite. *ACS Appl. Mater. Interfaces* **2017**, *9* (51), 44579−44583.
(19) Fu, P.; Huang, M.; Shang, Y.; Yu, N.; Zhou, H. L.; Zhang, Y. B.; Chen, S.; Gong, J.; Ning, Z. Organic-Inorganic Layered and Hollow Tin Bromide Perovskite with Tunable Broadband Emission. *ACS Appl. Mater. Interfaces* **2018**, *10* (40), 34363−34369.
(20) Wang, Z. P.; Wang, J. Y.; Li, J. R.; Feng, M. L.; Zou, G. D.; Huang, X. Y. [Bmim]2SbCl5: a main group metal-containing ionic liquid exhibiting tunable photoluminescence and white-light emission. *Chem. Commun.* **2015**, *51* (15), 3094−7.
(21) Zhou, C. K.; Worku, M.; Neu, J.; Lin, H. R.; Tian, Y.; Lee, S. J.; Zhou, Y.; Han, D.; Chen, S. Y.; Hao, A.; Djurovich, P. I.; Siegrist, T.; Du, M. H.; Ma, B. W. Facile Preparation of Light Emitting Organic Metal Halide Crystals with Near-Unity Quantum Efficiency. *Chem. Mater.* **2018**, *30* (7), 2374−2378.
(22) Zhou, C.; Lin, H.; Tian, Y.; Yuan, Z.; Clark, R.; Chen, B.; van de Burgt, L. J.; Wang, J. C.; Zhou, Y.; Hanson, K.; Meisner, Q. J.; Neu, J.; Besara, T.; Siegrist, T.; Lambers, E.; Djurovich, P.; Ma, B. Luminescent zero-dimensional organic metal halide hybrids with near-unity quantum efficiency. *Chem. Sci.* **2018**, *9* (3), 586−593.
(23) Adamo, C.; Barone, V. Toward reliable density functional methods without adjustable parameters: The PBE0 model. *J. Chem. Phys.* **1999**, *110* (13), 6158−6170.
(24) Muscat, J.; Wander, A.; Harrison, N. M. On the prediction of band gaps from hybrid functional theory. *Chem. Phys. Lett.* **2001**, *342* (3−4), 397−401.
(25) Giannozzi, P.; Andreussi, O.; Brumme, T.; Bunau, O.; Buongiorno Nardelli, M.; Calandra, M.; Car, R.; Cavazzoni, C.; Ceresoli, D.; Cococcioni, M.; Colonna, N.; Carnimeo, I.; Dal Corso, A.; de Gironcoli, S.; Delugas, P.; DiStasio, R. A.; Ferretti, A.; Floris, A.; Fratesi, G.; Fugallo, G.; Gebauer, R.; Gerstmann, U.; Giustino, F.; Gorni, T.; Jia, J.; Kawamura, M.; Ko, H. Y.; Kokalj, A.; Kucukbenli, E.; Lazzeri, M.; Marsili, M.; Marzari, N.; Mauri, F.; Nguyen, N. L.; Nguyen, H. V.; Otero-De-La-Roza, A.; Paulatto, L.; Ponce, S.; Rocca, D.; Sabatini, R.; Santra, B.; Schlipf, M.; Seitsonen, A. P.; Smogunov, A.; Timrov, I.; Thonhauser, T.; Umari, P.; Vast, N.; Wu, X.; Baroni, S. Advanced capabilities for materials modelling with Quantum ESPRESSO. *J. Phys.: Condens. Matter* **2017**, *29* (46), 465901.
(26) Thonhauser, T.; Zuluaga, S.; Arter, C. A.; Berland, K.; Schroder, E.; Hyldgaard, P. Spin Signature of Nonlocal Correlation Binding in Metal-Organic Frameworks. *Phys. Rev. Lett.* **2015**, *115* (13), 136402.
(27) Kresse, G.; Furthmüller, J. Efficient iterative schemes for ab initio total-energy calculations using a plane-wave basis set. *Phys. Rev. B: Condens. Matter Mater. Phys.* **1996**, *54* (16), 11169−11186.

https://dx.doi.org/10.1021/jacs.9b13772
J. Am. Chem. Soc. 2020, 142, 4242−4253

(28) Kresse, G.; Joubert, D. From ultrasoft pseudopotentials to the projector augmented-wave method. *Phys. Rev. B: Condens. Matter Mater. Phys.* **1999**, *59* (3), 1758−1775.
(29) Thonhauser, T.; Cooper, V. R.; Li, S.; Puzder, A.; Hyldgaard, P.; Langreth, D. C. Van der Waals density functional: Self-consistent potential and the nature of the van der Waals bond. *Phys. Rev. B: Condens. Matter Mater. Phys.* **2007**, *76* (12), 125112.
(30) Berland, K.; Cooper, V. R.; Lee, K.; Schroder, E.; Thonhauser, T.; Hyldgaard, P.; Lundqvist, B. I. van der Waals forces in density functional theory: a review of the vdW-DF method. *Rep. Prog. Phys.* **2015**, *78* (6), 066501.
(31) Langreth, D. C.; Lundqvist, B. I.; Chakarova-Kack, S. D.; Cooper, V. R.; Dion, M.; Hyldgaard, P.; Kelkkanen, A.; Kleis, J.; Kong, L.; Li, S.; Moses, P. G.; Murray, E.; Puzder, A.; Rydberg, H.; Schroder, E.; Thonhauser, T. A density functional for sparse matter. *J. Phys.: Condens. Matter* **2009**, *21* (8), 084203.
(32) Frisch, M. J.; Trucks, G. W.; Schlegel, H. B.; Scuseria, G. E.; Robb, M. A.; Cheeseman, J. R.; Scalmani, G.; Barone, V.; Petersson, G. A.; Nakatsuji, H.; Li, X.; Caricato, M.; Marenich, A. V.; Bloino, J.; Janesko, B. G.; Gomperts, R.; Mennucci, B.; Hratchian, H. P.; Ortiz, J. V.; Izmaylov, A. F.; Sonnenberg, J. L.; Williams; Ding, F.; Lipparini, F.; Egidi, F.; Goings, J.; Peng, B.; Petrone, A.; Henderson, T.; Ranasinghe, D.; Zakrzewski, V. G.; Gao, J.; Rega, N.; Zheng, G.; Liang, W.; Hada, M.; Ehara, M.; Toyota, K.; Fukuda, R.; Hasegawa, J.; Ishida, M.; Nakajima, T.; Honda, Y.; Kitao, O.; Nakai, H.; Vreven, T.; Throssell, K.; Montgomery, J. A., Jr.; Peralta, J. E.; Ogliaro, F.; Bearpark, M. J.; Heyd, J. J.; Brothers, E. N.; Kudin, K. N.; Staroverov, V. N.; Keith, T. A.; Kobayashi, R.; Normand, J.; Raghavachari, K.; Rendell, A. P.; Burant, J. C.; Iyengar, S. S.; Tomasi, J.; Cossi, M.; Millam, J. M.; Klene, M.; Adamo, C.; Cammi, R.; Ochterski, J. W.; Martin, R. L.; Morokuma, K.; Farkas, O.; Foresman, J. B.; Fox, D. J. *Gaussian 16*, rev. C.01; Gaussian Inc.: Wallingford, CT, 2016.
(33) Niu, Y.; Lee, J. K. pKa Prediction. In *Applied Theoretical Organic Chemistry*; World Scientific: 2017; pp 503−518.
(34) Frisch, M. J.; Trucks, G. W.; Schlegel, H. B.; Scuseria, G. E.; Robb, M. A.; Cheeseman, J. R.; Scalmani, G.; Barone, V.; Petersson, G. A.; Nakatsuji, H.; Li, X.; Caricato, M.; Marenich, A. V.; Bloino, J.; Janesko, B. G.; Gomperts, R.; Mennucci, B.; Hratchian, H. P.; Ortiz, J. V.; Izmaylov, A. F.; Sonnenberg, J. L.; Williams; Ding, F.; Lipparini, F.; Egidi, F.; Goings, J.; Peng, B.; Petrone, A.; Henderson, T.; Ranasinghe, D.; Zakrzewski, V. G.; Gao, J.; Rega, N.; Zheng, G.; Liang, W.; Hada, M.; Ehara, M.; Toyota, K.; Fukuda, R.; Hasegawa, J.; Ishida, M.; Nakajima, T.; Honda, Y.; Kitao, O.; Nakai, H.; Vreven, T.; Throssell, K.; Montgomery, J. A., Jr.; Peralta, J. E.; Ogliaro, F.; Bearpark, M. J.; Heyd, J. J.; Brothers, E. N.; Kudin, K. N.; Staroverov, V. N.; Keith, T. A.; Kobayashi, R.; Normand, J.; Raghavachari, K.; Rendell, A. P.; Burant, J. C.; Iyengar, S. S.; Tomasi, J.; Cossi, M.; Millam, J. M.; Klene, M.; Adamo, C.; Cammi, R.; Ochterski, J. W.; Martin, R. L.; Morokuma, K.; Farkas, O.; Foresman, J. B.; Fox, D. J. *Gaussian 09*, rev. A.02; Gaussian Inc.: Wallingford, CT, 2016.
(35) Albert, I. D. L.; Marks, T. J.; Ratner, M. A. Large Molecular Hyperpolarizabilities. Quantitative Analysis of Aromaticity and Auxiliary Donor-Acceptor Effects. *J. Am. Chem. Soc.* **1997**, *119* (28), 6575−6582.
(36) Chen, L.; Lin, C. C.; Yeh, C. W.; Liu, R. S. Light Converting Inorganic Phosphors for White Light-Emitting Diodes. *Materials* **2010**, *3* (3), 2172−2195.
(37) Ye, S.; Xiao, F.; Pan, Y. X.; Ma, Y. Y.; Zhang, Q. Y. Phosphors in phosphor-converted white light-emitting diodes Recent advances in materials, techniques and properties. *Mater. Sci. Eng., R* **2010**, *71* (1), 1−34.
(38) Hofbeck, T.; Monkowius, U.; Yersin, H. Highly efficient luminescence of Cu(I) compounds: thermally activated delayed fluorescence combined with short-lived phosphorescence. *J. Am. Chem. Soc.* **2015**, *137* (1), 399−404.
(39) Leitl, M. J.; Krylova, V. A.; Djurovich, P. I.; Thompson, M. E.; Yersin, H. Phosphorescence versus thermally activated delayed fluorescence. Controlling singlet-triplet splitting in brightly emitting and sublimable Cu(I) compounds. *J. Am. Chem. Soc.* **2014**, *136* (45), 16032−8.
(40) Hamze, R.; Peltier, J. L.; Sylvinson, D.; Jung, M.; Cardenas, J.; Haiges, R.; Soleilhavoup, M.; Jazzar, R.; Djurovich, P. I.; Bertrand, G.; Thompson, M. E. Eliminating nonradiative decay in Cu(I) emitters: > 99% quantum efficiency and microsecond lifetime. *Science* **2019**, *363* (6427), 601−606.
(41) Chandross, E. A.; Dempster, C. J. Intramolecular excimer formation and fluorescence quenching in dinaphthylalkanes. *J. Am. Chem. Soc.* **1970**, *92* (12), 3586−3593.
(42) Shen, Y.; Liu, H.; Cao, J.; Zhang, S.; Li, W.; Yang, B. Unusual temperature-sensitive excimer fluorescence from discrete pi-pi dimer stacking of anthracene in a crystal. *Phys. Chem. Chem. Phys.* **2019**, *21* (27), 14511−14515.
(43) Gao, Y.; Liu, H.; Zhang, S.; Gu, Q.; Shen, Y.; Ge, Y.; Yang, B. Excimer formation and evolution of excited state properties in discrete dimeric stacking of an anthracene derivative: a computational investigation. *Phys. Chem. Chem. Phys.* **2018**, *20* (17), 12129−12137.
(44) Kitada, N.; Ishida, T. Polymeric one- and two-dimensional copper(I) iodide complexes showing photoluminescence tunable by azaaromatic ligands. *CrystEngComm* **2014**, *16* (34), 8035−8040.
(45) *Dimethyl Sulfoxide Solubility Data*. Gaylord Chemical Company, L.L.C., https://www.gaylordchemical.com/literature/dmso-solubility-data/ (accessed Dec 21, 2019).
(46) Miyamae, H.; Numahata, Y.; Nagata, M. The Crystal-Structure of Lead(II) Iodide-Dimethylsulfoxide(1/2), PbI2(Dmso)2. *Chem. Lett.* **1980**, *9* (6), 663−664.
(47) Jeon, N. J.; Noh, J. H.; Kim, Y. C.; Yang, W. S.; Ryu, S.; Seok, S. I. Solvent engineering for high-performance inorganic-organic hybrid perovskite solar cells. *Nat. Mater.* **2014**, *13*, 897.
(48) Kobayashi, A.; Komatsu, K.; Ohara, H.; Kamada, W.; Chishina, Y.; Tsuge, K.; Chang, H. C.; Kato, M. Photo- and vapor-controlled luminescence of rhombic dicopper(I) complexes containing dimethyl sulfoxide. *Inorg. Chem.* **2013**, *52* (22), 13188−98.
(49) Stamplecoskie, K. G.; Manser, J. S.; Kamat, P. V. Dual nature of the excited state in organic-inorganic lead halide perovskites. *Energy Environ. Sci.* **2015**, *8* (1), 208−215.
(50) Sharenko, A.; Mackeen, C.; Jewell, L.; Bridges, F.; Toney, M. F. Evolution of Iodoplumbate Complexes in Methylammonium Lead Iodide Perovskite Precursor Solutions. *Chem. Mater.* **2017**, *29* (3), 1315−1320.
(51) Guo, Y.; Shoyama, K.; Sato, W.; Matsuo, Y.; Inoue, K.; Harano, K.; Liu, C.; Tanaka, H.; Nakamura, E. Chemical Pathways Connecting Lead(II) Iodide and Perovskite via Polymeric Plumbate(II) Fiber. *J. Am. Chem. Soc.* **2015**, *137* (50), 15907−14.

https://dx.doi.org/10.1021/jacs.9b13772
J. Am. Chem. Soc. 2020, 142, 4242−4253